



HAL
open science

Pisarenko Class Beamformer Applied to Passive Acoustic Mapping of Ultrasound Cavitation

Audrey Sivadon, Maxime Polichetti, Jean-Christophe Béra, François Varray,
Barbara Nicolas, Bruno Gilles

► **To cite this version:**

Audrey Sivadon, Maxime Polichetti, Jean-Christophe Béra, François Varray, Barbara Nicolas, et al..
Pisarenko Class Beamformer Applied to Passive Acoustic Mapping of Ultrasound Cavitation. Forum
Acusticum, Dec 2020, Lyon, France. pp.1061-1064, 10.48465/fa.2020.0397 . hal-03240246

HAL Id: hal-03240246

<https://hal.science/hal-03240246>

Submitted on 29 May 2021

HAL is a multi-disciplinary open access archive for the deposit and dissemination of scientific research documents, whether they are published or not. The documents may come from teaching and research institutions in France or abroad, or from public or private research centers.

L'archive ouverte pluridisciplinaire **HAL**, est destinée au dépôt et à la diffusion de documents scientifiques de niveau recherche, publiés ou non, émanant des établissements d'enseignement et de recherche français ou étrangers, des laboratoires publics ou privés.

PISARENKO CLASS BEAMFORMER APPLIED TO PASSIVE ACOUSTIC MAPPING OF ULTRASOUND CAVITATION

Audrey Sivadon¹ Maxime Polichetti¹ Jean-Christophe Béra¹
François Varray² Barbara Nicolas² Bruno Gilles¹

¹ Univ Lyon, Université Lyon 1, Inserm, LabTau, U1032,
151 cours Albert Thomas, 69003 Lyon, France

² INSA, Université Lyon 1, CNRS, CREATIS
7 avenue Jean Capelle, 69621 Lyon, France

audrey.sivadon@inserm.fr

1. INTRODUCTION

Ultrasound-induced cavitation used in therapeutic matters can be monitored using linear arrays and passive beamformers. The purpose of this monitoring is to localize accurately the cavitation clouds in the tissue during High Intensity Focused Ultrasound (HIFU) emission. The challenge is therefore to allow both high resolution of images and short time computation for real-time further applications of cavitation mapping. The state of the art, in Passive Cavitation Imaging (PCI) provides two approaches, each of them offering good results in one of the criteria mentioned above. In the Time Domain, the Robust Capon Beamformer (TD-RCB) [1–3] is an adaptive beamformer designed to reduce reconstruction artefacts. This method reveals results with high resolution and a good localization of the cavitation clouds but appears to be extremely time consuming. In the Fourier Domain, the non-adaptive Passive Cavitation Imaging (FD-PCI) [4–6] provides a time computation highly reduced and offers an additional advantage since it enables, through the choice of the frequency at which cavitation acoustic emissions are imaged, the differentiation of cavitation regimes. However, PCI shows low resolution images with non-negligible secondary lobes which alter the localization of cavitation.

Stoica has introduced an adaptive beamformer using Pisarenko's framework [7–9]. This method expresses the power spectrum of the signal radiated as a function of the estimated covariance matrix of the data with an adaptive parameter r . The Pisarenko class of methods allows a generic way to bring together two already existing beamformers depending on the value of the parameter r , non-adaptive Passive Acoustic Mapping (PAM) and Capon beamformer, corresponding respectively to $r = 1, -1$. In this paper, the focus will be on the study of Pisarenko beamformer with $r \geq 0$ and a particular interest will be given to the case $r = 0$ also called the MidWay (MW) approach for its intermediate abilities between complexity and resolution. The algorithm performances will be compared to those of FD-PCI and TD-RCB in order to show the benefits of this reconstruction method in terms of cavitation map quality and computation time.

2. PISARENKO CLASS OF METHODS

2.1 Implementation of Pisarenko beamformers in the Fourier Domain

The beamforming method illustrated in this paper employs a frequency domain approach by means of the Cross-Spectral Matrix (CSM) [10, 11].

Let us consider a linear array of N sensors and $\mathbf{y}(t)$ a matrix containing the time samples of each sensor with $\mathbf{Y}(f)$ its Fourier transform. With T the recording time, the $(N \times N)$ CSM ($M(f)$) associated with $\mathbf{Y}(f)$ is

$$\mathbf{M}(f) = E \left\langle \lim_{T \rightarrow +\infty} \frac{1}{T} \mathbf{Y}(f) \mathbf{Y}^*(f) \right\rangle, \quad (1)$$

where $E \langle \rangle$ and $()^*$ denote respectively the expectation and conjugate transpose. The CSM being the frequency equivalent of the Covariance Matrix, this formulation allows the use of many adaptive methods such as Pisarenko Beamformer introduced by Stoica [7, 8] in the frequency domain (FD-PISA). We can therefore express the power of the source as a function of space \vec{r} at the frequency f as

$$\hat{\mathbf{P}}(\vec{r}, f) = \begin{cases} [\mathbf{h}^* (\hat{\mathbf{M}})^r \mathbf{h}]^{1/r} & \text{for } r \neq 0 \\ \exp[\mathbf{h}^* \ln(\hat{\mathbf{M}}) \mathbf{h}] & \text{for } r = 0 \end{cases}; \quad (2)$$

with $\mathbf{h}(f)$ being the steering vector and $r \in [0, 1]$ the adaptive parameter. The definition for $r = 0$ is actually the limit solution of the general expression for $r \neq 0$. Let us denote $\hat{\mathbf{P}}$ and $\hat{\mathbf{M}}$ respectively the power and CSM estimates. The CSM estimation is a critical step towards high quality maps. The approach adopted here consists in partitioning the temporal data representing artificial realizations of duration T_{snap} and averaging on the number of $Y_k(f)$, K , as follows :

$$\hat{\mathbf{M}}(f) = \frac{1}{T_{snap}} \frac{1}{K} \sum_{k=1}^K \mathbf{Y}_k(f) \mathbf{Y}_k^*(f), \quad (3)$$

where K is chosen larger than the number of sensors in the array.

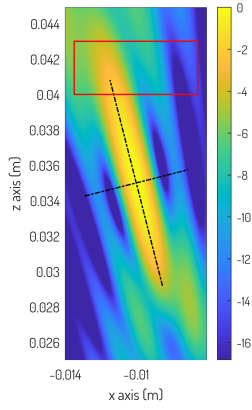


Figure 1. Normalised power map with the axial and lateral axes used to compute the respective resolutions and the artifact region used to compute the CAR.

2.2 Study of the adaptive parameter r and MidWay approach

2.2.1 Method

The simulated probe is composed of 128 elements along the x axis, centered at $x = 0$ and $z = 0$ with 0.3 mm spacing between elements. Its center frequency is 4 MHz and its bandwidth at -6 dB is $[0.5 - 8]$ MHz. The signal is a punctual harmonic source with fundamental frequency 1 MHz positioned 10 mm away from the probe's center along the x axis and 35 mm along the z axis (depth). Additional noise is added in post-processing with a Signal-to-Noise-Ratio (SNR) of 10 dB to simulate acquisition noise.

The reconstruction plan is the $x - z$ plan. We compute the fundamental frequency of the harmonic source and vary the parameter r in the reconstruction algorithm in order to study its influence on the power maps.

In order to have quantified comparison, the axial and lateral resolutions at -3 dB and the Cavitation-to-Artifact Ratio (CAR) are computed. The axial and lateral -3 dB resolutions are obtained using axes taken along the ellipse-like main lobe (Figure 1), and CAR corresponds to the ratio

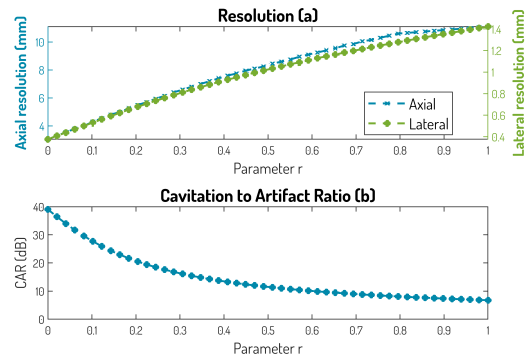


Figure 3. (a) Resolution values at -3 dB as a function of the parameter r for the axial and lateral axes of the main lobe. (b) Cavitation to Artefact Ratio values as a function of the parameter r .

between the average level of pixels respectively in the cavitation (μ_{cav}) and in the artifact (μ_{art}) regions (see Figure 1) as :

$$CAR = 10 \log_{10} \left(\frac{\mu_{cav}}{\mu_{art}} \right). \quad (4)$$

In the present case, cavitation is represented by a punctual source. Therefore, the cavitation region is reduced to one pixel at the source position.

2.2.2 Results and Discussion

On Figure 2, the normalised power maps obtained with r ranging from 1 to 0 from left to right are presented. The case $r = 1$ presents a large main lobe and sidelobes at approximately -10 dB along the lateral axis (orthogonal to the main axis of the ellipse-like main lobe) and up to -5 dB closer to axial edges of the main lobe. The size of the main lobe and the amplitudes of the sidelobes tend to decrease while r goes to 0. Indeed, the normalised power map for the MW approach presents no sidelobes above -30 dB and much reduced size of the main lobe.

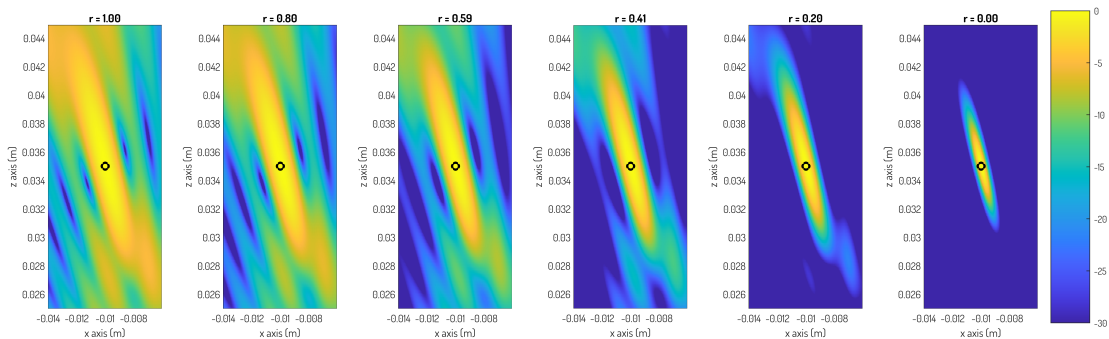


Figure 2. Normalised power maps at -30 dB in the $x - z$ plan at 1 MHz. The parameter r evolves from 1 to 0 from left to right. The maps for $r \neq 0$ and $r = 0$ corresponds respectively to the Pisarenko class and the MW approach with expressions (2). The black circle determines the ground truth position of the source. The resolution of the reconstructed plan is $\delta x = 0.04$ mm and $\delta z = 0.1$ mm.

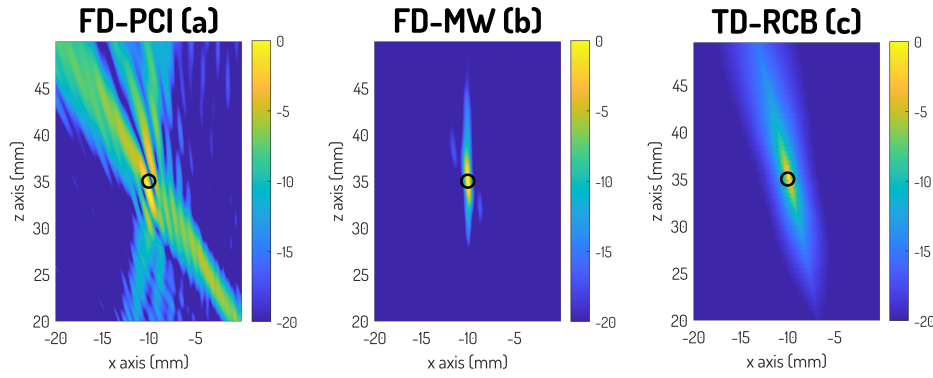


Figure 4. Normalised power maps at -20 dB in the $x - z$ plan. (a) Reconstruction at 2.5 MHz using FD-PCI algorithm. (b) Reconstruction at 2.5 MHz using FD-MW (Pisarenko with $r = 0$). (c) Reconstruction using TD-RCB algorithm with $\epsilon = 0.01$. The resolution of the reconstructed plan is $\delta x = 0.02$ mm and $\delta z = 0.05$ mm for the frequency domain computation and $\delta x = 0.2$ and $\delta z = 0.5$ mm for the time domain computation. The black circles determine the actual position of the source.

On the top panel of Figure 3, the resolution is presented for both axial and lateral axes as a function of the parameter r . The evolution of the resolution is similar for both axes decreasing towards the MW value, 75% under the $r = 1$ value. On the lower panel of Figure 3, the CAR is plotted as a function of r . It tends to grow until a limit value corresponding to the MW approach, 5 times the CAR of $r = 1$.

Regarding these results concerning the influence of the adaptive parameter r , the MW approach seems to be the most relevant case of Pisarenko class, with the additional benefit of being a parameter-free method. From now on, the Pisarenko class will be computed only for $r = 0$ and called MidWay (FD-MW).

3. COMPARISON OF FD-MW WITH FD-PCI AND TD-RCB

3.1 Method

In order to compare the three methods regarding their application to ultrasound-induced cavitation imaging, we choose to simulate inertial cavitation using a white Gaussian noise. The position of the source and the probe are kept as in the previous part. The power radiated has been estimated, in the time domain, using TD-RCB with $\epsilon = 0.01$, and in the frequency domain, FD-PCI along with FD-MW at 2.5 MHz. The resulted power maps are presented on Figure 4. The resolution and CAR were computed and displayed on Figure 5 with an artifact region (see equation 4) defined by $x \in [-19; -2]$ mm and $z \in [41; 46]$ mm.

3.2 Results and Discussion

The left panel of Figure 4 reveals the X-shape, very common to PAM beamformers, that the adaptive beamformers aim to reduce. The power maps on panels (b) and (c) of Figure 4 indeed show a better localisation of the source with no sidelobes and a resolution much smaller than with

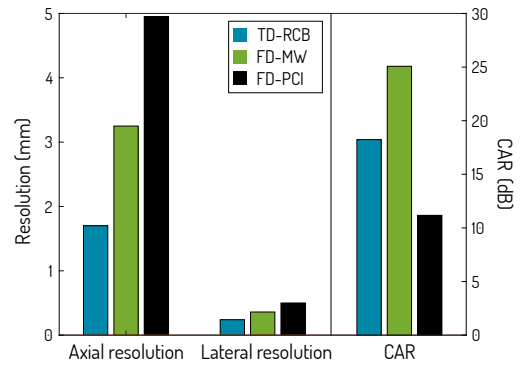


Figure 5. Resolution and CAR for power maps of figure 4.

non-adaptive FD-PCI method. Apart from the fact that lateral resolution is about 7 times better than axial one, which is typical of passive imaging, Figure 5 shows that the resolution of FD-MW is between the ones of TD-RCB and FD-PCI. However, the CAR is better with FD-MW than with the two classical methods. In terms of cavitation mapping quality (resolution and artefact), the FD-MW method presents itself as a good compromise between FD-PCI and TD-RCB.

Considering now the computation time, the duration of each map reconstruction was measured for each algorithm. Let us preliminarily remind that the values presented can vary depending on the computer's capabilities and are given only as a matter of comparison. The computer used is composed of an Intel(R) Core(TM) i7 processor¹ with 16 Go RAM memory and a windows 10, 64 bits operating system. The time computations are 14 s, 17 s and 22 min respectively for FD-PCI, FD-MW and TD-RCB, reminding that the resolution of the reconstruction space for the Time Domain computation is 10 times lower

¹ Interl(R) Core(TM) i7-8665U CPI @ 1, 90 GHz and 2, 11 GHz

that the one for the Frequency Domain. The Frequency Domain computation, with equivalent times for FD-PCI and FD-MW, presents a drastic reduce being only 1% of the Time Domain computation and the adaptive MW algorithm allows a better resolution with no sidelobes and a good contrast.

Finally, on Figure 4, the real positions of the source is displayed with black circles and FD-PCI reveals a small error compared to the two adaptive methods FD-MW and TD-RCB. This final observation supports once again the Frequency Domain MidWay Approach.

4. CONCLUSIONS

In this paper, the use of the Pisarenko Beamformer for Passive Cavitation Imaging has been presented in the Fourier Domain using the Cross-Spectral Matrix (CSM) formulation. This allows a large reduction of time computation, compared to the time domain reconstruction algorithms such as TD-RCB. The limit of $r = 0$, called MidWay approach (FD-MW) appears to be the most relevant case of Pisarenko Beamformer, being a parameter-free adaptive method with the best abilities in terms of cavitation map quality (resolution and contrast). Moreover, FD-MW is presented here as a good compromise between image quality and time cost, with resolution and artifact reduction significantly better than FD-PCI. Though, the simulations presented in this paper are very simple ways of defining cavitation activity which is a much more complicated phenomenon. Two aspects can be investigated, the first one lies on the experimental use of Pisarenko's Beamformer to ensure its capabilities on real cavitation signals and the second one concerns the research of a more complete simulation of cavitation clouds with multiple sources.

5. REFERENCES

- [1] P. Stoica, Z. Wang, and J. Li, "Robust capon beamforming," in *Conference Record of the Thirty-Sixth Asilomar Conference on Signals, Systems and Computers, 2002.*, vol. 1, pp. 876–880, IEEE, 2002.
- [2] J. Li, P. Stoica, and Z. Wang, "On robust capon beamforming and diagonal loading," *IEEE transactions on signal processing*, vol. 51, no. 7, pp. 1702–1715, 2003.
- [3] C. Coviello, R. Kozick, J. Choi, M. Gyöngy, C. Jensen, P. P. Smith, and C.-C. Coussios, "Passive acoustic mapping utilizing optimal beamforming in ultrasound therapy monitoring," *The Journal of the Acoustical Society of America*, vol. 137, no. 5, pp. 2573–2585, 2015.
- [4] K. J. Haworth, K. B. Bader, K. T. Rich, C. K. Holland, and T. D. Mast, "Quantitative frequency-domain passive cavitation imaging," *IEEE transactions on ultrasonics, ferroelectrics, and frequency control*, vol. 64, no. 1, pp. 177–191, 2016.
- [5] K. J. Haworth, T. D. Mast, K. Radhakrishnan, M. T. Burgess, J. A. Kopechek, S.-L. Huang, D. D. McPherson, and C. K. Holland, "Passive imaging with pulsed ultrasound insonations," *The Journal of the Acoustical Society of America*, vol. 132, no. 1, pp. 544–553, 2012.
- [6] V. A. Salgaonkar, S. Datta, C. K. Holland, and T. D. Mast, "Passive cavitation imaging with ultrasound arrays," *The Journal of the Acoustical Society of America*, vol. 126, no. 6, pp. 3071–3083, 2009.
- [7] P. Stoica, J. Li, and X. Tan, "On spatial power spectrum and signal estimation using the pisarenko framework," *IEEE Transactions on Signal Processing*, vol. 56, no. 10, pp. 5109–5119, 2008.
- [8] L. Du, T. Yardibi, J. Li, and P. Stoica, "Review of user parameter-free robust adaptive beamforming algorithms," *Digital Signal Processing*, vol. 19, no. 4, pp. 567–582, 2009.
- [9] V. Pisarenko, "On the estimation of spectra by means of non-linear functions of the covariance matrix," *Geophysical Journal International*, vol. 28, no. 5, pp. 511–531, 1972.
- [10] J. Maksym, "A robust formulation of an optimum cross-spectral beamformer for line arrays," *The Journal of the Acoustical Society of America*, vol. 65, no. 4, pp. 971–975, 1979.
- [11] D. E. Grant, J. H. Gross, and M. Zebrick Lawrence, "Cross-spectral matrix estimation effects on adaptive beamforming," *The Journal of the Acoustical Society of America*, vol. 98, no. 1, pp. 517–524, 1995.